



OPEN

Towards optimization of plant cell detection in suspensions using impedance-based analyses and the unified equivalent circuit model

Kian Kadan-Jamal^{1,5✉}, Aakash Jog^{2,5}, Marios Sophocleous^{2,3}, Julius Georgiou³, Adi Avni⁴ & Yosi Shacham-Diamand^{1,2}

An improved approach for comparative study of plant cells for long term and continuous monitoring using electrical impedance spectroscopy is demonstrated for tomato and tobacco plant cells (MSK8 and BY2) in suspensions. This approach is based on the locations and magnitudes of defining features in the impedance spectra of the recently reported unified equivalent circuit model. The ultra-wide range (4 Hz to 20 GHz) impedance spectra of the cell lines were measured using custom probes, and were analyzed using the unified equivalent circuit model, highlighting significant negative phase peaks in the ~1 kHz to ~10 MHz range. These peaks differ between the tomato and tobacco cells, and since they can be easily defined, they can potentially be used as the signal for differentiating between different cell cultures or monitoring them over time. These findings were further analysed, showing that ratios relating the resistances of the media and the resistance of the cells define the sensitivity of the method, thus affecting its selectivity. It was further shown that cell agglomeration is also an important factor in the impedance modeling in addition to the overall cell concentration. These results can be used for optimizing and calibrating electrical impedance spectroscopy-based sensors for long term monitoring of cell lines in suspension for a given specific cell and media types.

The global population is expected to exceed 9 billion by 2050, demanding an increase in food production by approximately 70%^{1,2}. However, while the population increases, the arable land size is gradually decreasing, further aggravating the need for more efficient agricultural methods^{3–5}. Monitoring methods for use in precision agriculture are necessary to balance the increasing demands and the reducing land availability^{6–8}. In order to achieve sustainability, it is important to gather data and monitor farming parameters such as soil quality, plants, crops and other environmental parameters^{9–16}. Data driven agriculture requires research and development of low-cost, field-deployable sensors that can be easily interfaced to the internet and Internet of Things (IoT) compatible¹⁷. Therefore, electrical sensors with low-cost electronics, which can be mass produced, are being investigated.

One family of such sensors is based on Electrical Impedance Spectroscopy (EIS), and uses commonly available impedance measurement systems. EIS has been widely used in biomedical applications^{18,19}, with a variety of cells and tissues. Thus, there exists a very thorough background for this technique, both in theory and in practice. In particular, EIS can be used in the field of agriculture and food, for assessment of plant cell and tissue conditions^{20–24}. The EIS spectra of the plant cell or tissue can be represented by an equivalent electrical circuit, using lumped components. The electrical topology of such a model can be decided arbitrarily based on optimal fitting, or be based on the physical properties and the macro and micro structures of the cells, tissues, and organs^{25,26}. The impedance spectra of plant cells are affected by physical parameters of the cells, such as the

¹Department of Materials Science and Engineering, Faculty of Engineering, Tel Aviv University, 69978 Tel Aviv, Israel. ²Department of Physical Electronics, School of Electrical Engineering, Faculty of Engineering, Tel Aviv University, 69978 Tel Aviv, Israel. ³Department of Electrical and Computer Engineering, EMPHASIS Research Center, University of Cyprus, 1678 Nicosia, Cyprus. ⁴School of Plant Sciences and Food Security, Tel-Aviv University, Tel Aviv, Israel. ⁵These authors contributed equally: Kian Kadan-Jamal and Aakash Jog. ✉email: kiankadan@mail.tau.ac.il

shape of the cells, electrical properties of the cell wall, plasma membranes, cytoplasm, and intra and extracellular conductivities^{27,28}. Additionally, EIS can be used to demonstrate a close relationship between the dielectric properties of suspended cells, like capacitance, and its biomass concentration^{29–31}. EIS can also be used to estimate the thickness of the cell wall and plasma membrane by properly modelling the various volume fractions of the cell suspensions^{21,27,28,32}. A unified equivalent circuit model for plant cells has been recently reported^{33,34} for an ultra-wide frequency range (4 Hz–20 GHz). The unified model was used to fit experimentally obtained EIS spectra of tomato cells (MSK8) in Murashige and Skoog (MS) media. However, further investigation into the dependence of this method on the properties of the cells and media is required. Although the reported equivalent circuit model has been shown to provide accurate fits to the measurements, the way to use that model is not investigated. In order for that model to become useful in real-time monitoring of plant health, the relationships between the model's components with plant physiology should be identified in a systematic manner.

Hence, a novel study on two different cell types in two different media has been presented in this work. This work attempts to build the foundations for relating the parameter variations of the model with plant physiological changes but also looking into how those relationships can change from one type of plant to another. Furthermore, this work is an attempt to show that optimization of monitoring parameters is feasible by varying specific media parameters. Suspensions of tomato cells (MSK8) and tobacco cells (BY2) in Murashige and Skoog (MS) and phosphate buffer (PB) media were studied. The experimentally observed spectra were fitted to the unified model. Although all data exhibited a good fitting with the model, a few fundamental differences were observed in the measurements in the range of ~1 kHz to ~10 MHz. The most pronounced differences were those in the height and locations of peaks in the phase spectra. Therefore, a new analytical approach for characterization of the concentration and type of cells in a cell suspension, has been proposed. This approach is based on the locations and heights of peaks in the phase of the impedance spectra, and the heights of plateaus in the gain of the impedance spectra. The theoretical analyses are presented and discussed critically, and are applied to the experimentally obtained data in order to demonstrate their efficacy with regards to discrimination between cell and medium types.

Materials and methods

Preparation and analysis of cells. *Cell cultures.* Tomato (*S. lycopersicum* cv Mill; line MSK8³⁵) and tobacco (*N. tabacum* cv BY2³⁶) cell suspension cultures were grown in Murashige and Skoog (MS)³⁷ media including vitamins (Duchefa Biochemie) in 250 mL flask with 100 mL liquid, supplemented with 30 g/L sucrose, 1 mg/L 2,4-dichlorophenoxyacetic acid (2,4-D) and 0.1 mg/L kinetin, which was set to pH 5.7. Both cell lines were prepared and grown in-house at the School of Plant Sciences and Food Security, Tel Aviv University, following standard procedures^{35,36}. The cell cultures were centrifuged at 25 °C in the dark, at approximately 100 rpm. Sub-culturing was performed every 2 weeks. MSK8 cells were used 14–20 days after sub-culturing and BY2 cells were used 4–6 days after weekly sub-culturing. The cells samples were diluted before the experiment in fresh MS or PB media [0.1 M] at pH 5.8³³.

EIS measurements. EIS measurements were carried out in the frequency range of 4 Hz to 20 GHz using multiple instruments. More details about the setup and tools used, and their error margins can be found in³⁴. For each experiment, cells were filtered out from the growth media, and then re-suspended in fresh media before the beginning of each measurement. The suspensions were diluted down to the required concentrations using fresh media. All measurements were performed at room temperature (25 °C). Each experiment was repeated 3–5 times, and the differences between the obtained impedance spectra were observed to be well within the error margins of the equipment used³³.

Results and discussion

Electrical modelling. Based on previously published works, the cell suspensions can be modelled using the unified Randles–Debye model (see Fig. 1)³³. In this model, R_s , R_{ct} , C_{dl} , and the CPE as are defined in a standard Randles model, R represents the resistance of the cells, R_1 represents the resistance of the solution, C represents the capacitance due to the presence of cells in the suspension, and C_1 represents the capacitive effects of water polarization.

An impedance spectrum obtained from the simplified version of the unified Randles–Debye model, consists of three distinct dispersions corresponding to the three capacitors C_{dl} , C , and C_1 . Of these, the first represents the double layer capacitance and the remaining two represent the imaginary parts of the Debye dispersion due to dielectric relaxation at high frequencies. Each dispersion can be represented by a simple rational first order polynomial function with one pole and one zero, such that the pole frequency is less than that of the zero. Hence, these dispersions correspond to 3 poles and 3 zeroes, thus creating 7 regions in the impedance spectrum. For the sake of simplicity, the Warburg element in the Randles model has been ignored in this analysis since it only comes into effect at very low frequencies (i.e. below the lowest studied frequency of 4 Hz). The analysis uses the notation ω_{ij} to denote the corner angular frequency (either corresponding to a pole or to a zero) between regions i and j . The angular frequency is related to the frequency as $\omega_{ij} = 2\pi f_{ij}$.

Figure 2 shows the asymptote-based impedance magnitude spectrum of the unified equivalent circuit model on logarithmic axes³³. Region 1 corresponds to the lowest range of frequencies, in which all three capacitors have very high impedance (relative to their components in parallel with them). Hence, the magnitude of the impedance is approximately $R_s + R_{ct} + R_1$. The first pole, at the angular frequency ω_{12} , is determined by the largest capacitor, i.e. C_{dl} . Hence, the pole occurs at the frequency at which the impedance of C_{dl} matches $R_s + R_{ct} + R_1$.

In region 2, the charge transfer resistance (R_{ct}) in the Randles model is shunted by the double layer capacitance (C_{dl}). In this region, the magnitude of the impedance falls at a rate of –20 dB/dec. The zero due to C_{dl}

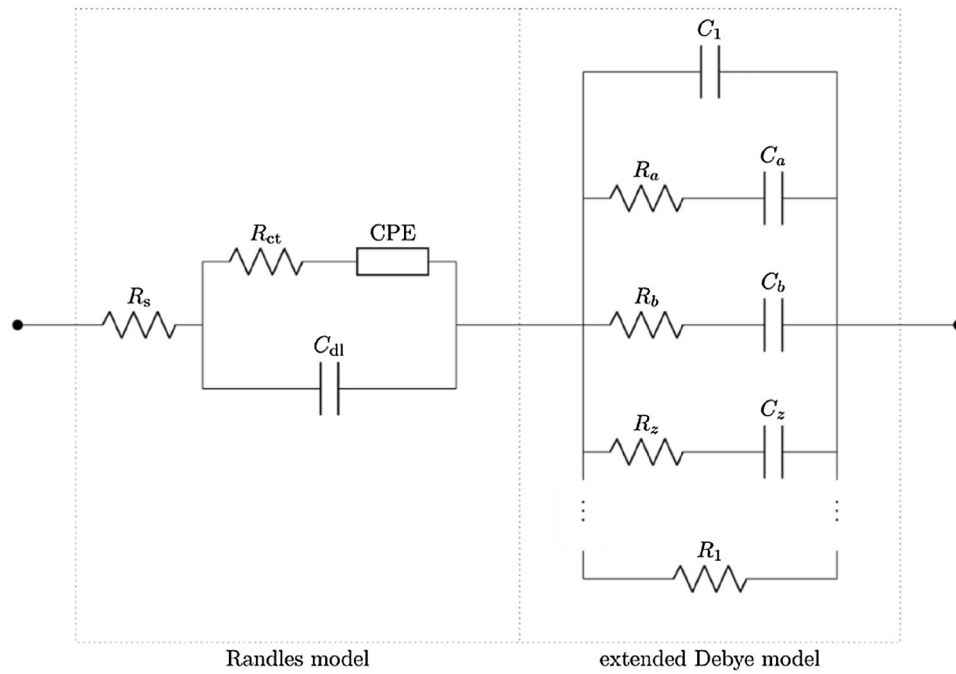


Figure 1. The unified equivalent circuit model of the cell-line suspension, and in the extended Debye model section³³.

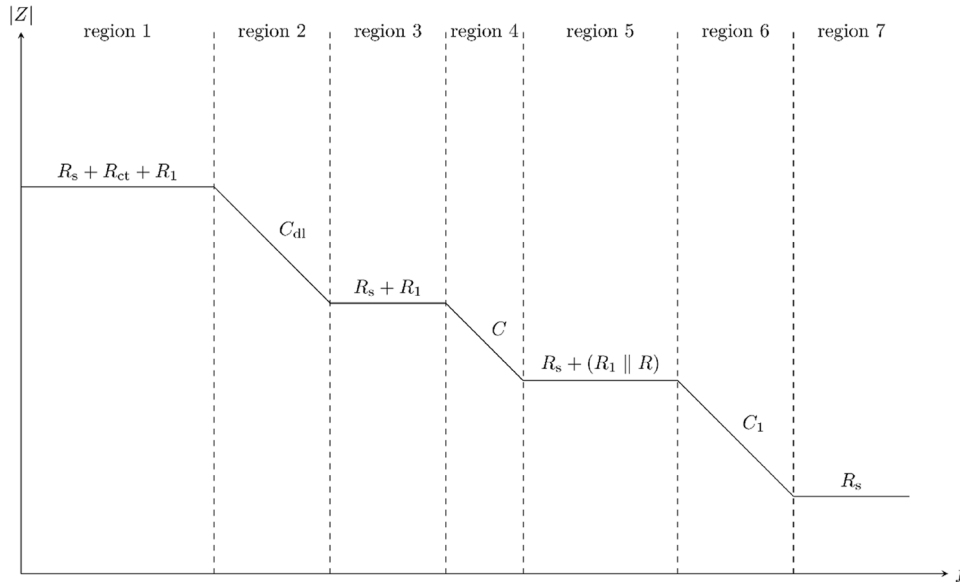


Figure 2. A schematic drawing based on the asymptote-based approximation of the impedance spectra of the simplified unified equivalent circuit model for cell suspensions.

corresponds to the frequency at which the impedance, corresponding to the double layer capacitance, becomes negligibly small compared to $R_s + R_1$.

The second-largest capacitor, i.e. C_3 , behaves in the opposite manner. Its impedance comes into effect once it becomes comparable to $R_s + R_1$, i.e. beyond ω_{34} . Once the magnitude of its impedance drops to a sufficiently small value, the impedance of the R-C branch in the Debye model is governed by R . Hence, in region 5, the magnitude of the impedance is approximately $R_s + R_1 \parallel R$.

The smallest capacitor, i.e. C_1 , behaves in a manner similar to C_{dl} , by shunting the other branches of the Debye model. The frequencies and impedance magnitudes corresponding to the poles and zeros are as in Table S1. The frequency dependence of each dispersion can be described using a bilinear complex function $\frac{1+j\frac{\omega}{\omega_{zero}}}{1+j\frac{\omega}{\omega_{pole}}}$ where

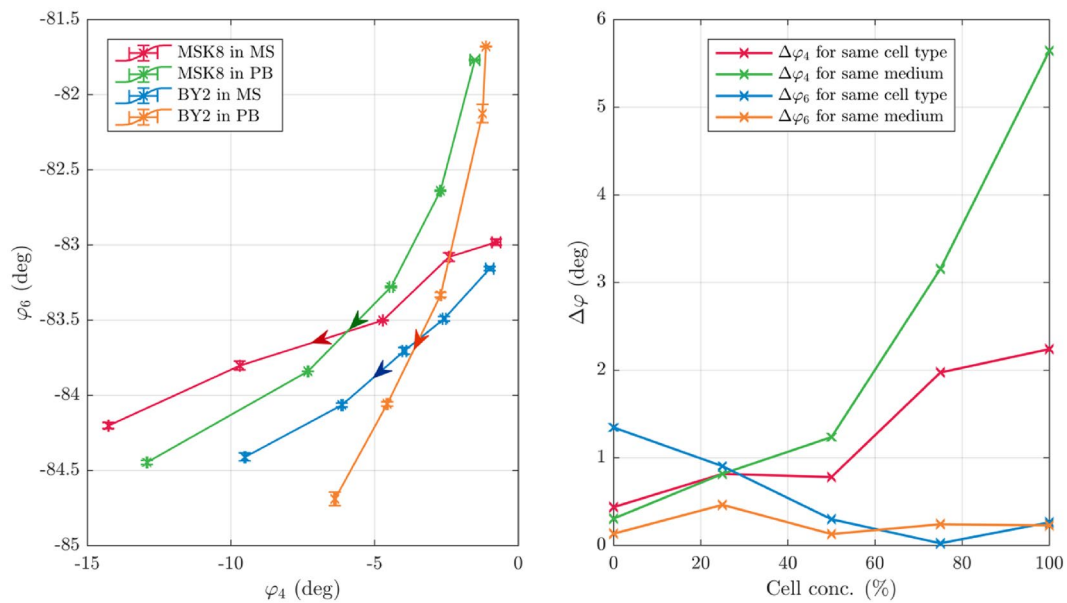


Figure 3. (left) φ_4 vs φ_6 for all four suspensions across the entire range of cell concentration, with the arrows indicating increasing cell concentration, and error bars indicating min–max bounds (right) mean deviation in φ_4 ($\Delta\varphi_4$) for all pairs of suspensions with the same cell-type, and for all pairs of suspensions with the same media.

ω_{pole} , the angular frequency corresponding to the pole, is smaller than ω_{zero} , the angular frequency corresponding to the zero. On a logarithmic frequency axis, the phase of this bilinear complex function has a bell-shape, with the negative phase peak occurring at a frequency which is the geometric mean of the pole and zero frequencies, i.e. $\omega_{\text{peak}} = \sqrt{\omega_{\text{pole}} \cdot \omega_{\text{zero}}}$. Thence, the minimum phase (i.e. the phase at ω_{peak}), is determined by:

$$\omega_{\text{min phase}} = \arctan \left(\sqrt{\frac{\omega_{\text{pole}}}{\omega_{\text{zero}}}} \right) - \arctan \left(\sqrt{\frac{\omega_{\text{zero}}}{\omega_{\text{pole}}}} \right) \quad (1)$$

Therefore, the negative phase peaks in regions 4 and 6 correspond to the frequency pairs (ω_{34}, ω_{45}) and (ω_{56}, ω_{67}), respectively. Henceforth, the negative phase peaks in regions 4 and 6 are referred to as φ_4 and φ_6 , respectively, and the frequencies corresponding to these peaks are referred to as f_4 and f_6 , respectively.

The experimentally obtained impedance spectra for all combinations of cells and media were fitted to the unified equivalent circuit model (see Fig. 3)³³. The locations and heights of the two aforementioned phase peaks were calculated based on the fitted parameters and the above analytically obtained expressions. In order to study the impact of cell and medium type on φ_4 and φ_6 , the two were plotted against each other, for all four combinations of cell types and media.

Figure 3 (left) shows φ_4 and φ_6 , derived from the experimental spectra, for all four suspensions across the entire range of cell concentration. As expected based on previous work³³, suspensions with higher concentrations have larger negative phase peaks, i.e. higher φ_4 and φ_6 . Moreover, for low cell concentrations, the minimum phases for a given suspension are closer to those for suspensions with the same media type (e.g. MSK8 in MS and BY2 in MS). Conversely, for high cell concentrations, the minimum phases are closer for suspensions with the same cell type (e.g. MSK8 in MS and MSK8 in PB).

Figure 3 (right) shows the mean deviation in φ_4 ($\Delta\varphi_4$) for all pairs of suspensions with the same cell-type, and for all pairs of suspensions with the same media. As the concentration of cells in the suspensions increases, $\Delta\varphi_4$ increases for both of types of neighbors. However, the values and rate of increase in $\Delta\varphi_4$ for suspensions with the same media are much larger than that for suspensions with the same cell-type. This is consistent with the expectation that φ_4 is determined primarily by the cells (and not the media), and thence the deviation in φ_4 should be lower for suspensions consisting of the same cell type³³.

In order to further analyze these behaviors, an analytical approach was adopted.

Mathematical modelling and detection optimization. The impedance spectra—and hence the extracted parameters corresponding to the phase peaks and magnitude plateaus—depend not only on the absolute values of the resistances in the unified model, but also on the ratio between them.

Therefore, in order to analyze the dependence on these ratios, let $R = kR_1$ and let $R_s = pR_1$. Hence, ω_4 and ω_6 vary with k and p according to:

$$\omega_4 = \frac{1}{CR_1} \sqrt{\frac{1}{k(k+1)}} \quad (2)$$

$$\omega_6 = \frac{1}{C_1 R_1} \sqrt{\frac{1}{p\left(p + \frac{k}{k+1}\right)}} \quad (3)$$

Similarly, φ_4 and φ_6 vary with k and p according to:

$$\varphi_4 = \arctan\left(\sqrt{\frac{k}{k+1}}\right) - \arctan\left(\sqrt{\frac{k+1}{k}}\right) \quad (4)$$

$$\varphi_6 = \arctan\left(\sqrt{\frac{p}{p + \frac{k}{k+1}}}\right) - \arctan\left(\sqrt{\frac{p + \frac{k}{k+1}}{p}}\right) \quad (5)$$

Both φ_4 and φ_6 are independent of the capacitances C and C_1 , and depend only on the ratios of the resistances. In particular, for an infinitesimally small k , i.e. if R is significantly smaller than R_1 , then φ_4 approaches -90° . However, practically for most cell types and media, R is larger than R_1 . Hence, φ_4 is bounded by approximately -20° from below.

Similarly, as R_s is orders of magnitude smaller than R_1 , φ_6 is close to -90° (and in particular is bounded from above by approximately -74° for $k = 1$ and $p = 0.01$).

Based on the above equations, φ_4 depends only on k , whilst the capacitance due to the cells only affects f_4 . It would have been expected that f_4 would be proportional to the concentration of the cells. However, Figure S7 (left) shows that the relationship is somewhat random for f_4 whereas Figure S7 (right) shows that there exists a much clearer relationship between f_6 and the cell concentration. The microscopic images of the cells shown in Figures S6 show that cells agglomerate significantly, an effect that has a more significant influence on the capacitance compared to the effect of concentration. On the other hand, f_6 shows as much clearer relationship on the cell concentration since it depends mostly on the effect of the media (MS or PB).

Therefore, in order to amplify the effects of cell concentration on φ_4 , k should be as small as possible, i.e. R should be as close to or smaller than R_1 . Solving with k and p as above, the magnitude of the impedance in region 5 is:

$$|Z|_5 = R_1 \left(p + \frac{k}{k+1} \right) \quad (6)$$

For a given cell suspension, the deviation in $|Z|_5$ with respect to the medium is defined by:

$$d = \frac{|Z|_{5\text{suspension}}}{|Z|_{5\text{medium}}} \quad (7)$$

Hence, in order to amplify the effects of cell concentration on $|Z|_5$, d should be as large as possible. As d is inversely proportional to $|Z|_{5\text{medium}}$, the deviation is higher for media with lower conductivity, as shown in Fig. 4. This is consistent with the spectra in Figures S1–S5, where the deviation is larger for PB than for MS.

Conclusions

In this work, the effect of cell concentrations, cell types and media types of cell suspensions in an ultra-wide frequency range (4 Hz–20 GHz) has been investigated both experimentally and mathematically. The analysis is based on the recently published unified model^{33,34}. It was found that as the cell concentration increases, the magnitude of the negative phase peaks (φ_4 and φ_6) increase. Additionally, as the cell concentration decreases, the minimum phases for a given suspension tend to converge to the intrinsic behavior of the media. Conversely, as the cell concentration increases, the minimum phases converge to the intrinsic behavior of the cells. Furthermore, it was found that φ_4 is determined primarily by the cells (and not the media), and thence the deviation in φ_4 should be lower for suspensions consisting of the same cell type.

It has been mathematically modelled and shown that following the simplified unified impedance model, both φ_4 and φ_6 are independent of the capacitances C and C_1 , and depend only on the ratios of the resistances. For an infinitesimally small k , φ_4 approaches -90° but practically for most cell types and media, R is larger than R_1 . Hence, φ_4 is bounded by approximately -20° from below. Similarly, as R_s is orders of magnitude smaller than R_1 , φ_6 is close to -90° (and in particular is bounded from above by approximately -74° for $k = 1$ and $p = 0.01$). Hence, as the scope for improvement is limited by these bounds, in an ideal and best-case scenario, there is room for a $10\times$ improvement in the sensitivity.

It was further shown that φ_4 depends only on k , whilst the capacitance due to the cells only affects f_4 . It would have been expected that f_4 would be proportional to the concentration of the cells however, it is found that cell agglomeration has a more significant influence on the capacitance compared to the effect of concentration. On the other hand, f_6 shows a much clearer relationship on the cell concentration since it depends mostly on the effect of the media (MS or PB). Therefore, in order to amplify the effects of cell concentration on φ_4 , k should be

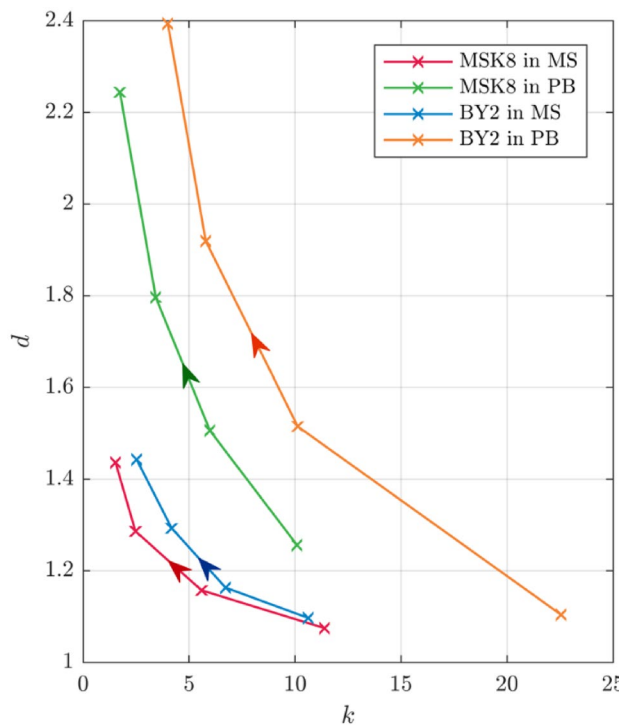


Figure 4. The relationship between d and k for various cell concentrations in both media for both cell types, with the arrows indicating increasing cell concentration.

as small as possible. Additionally, in order to amplify the effects of cell concentration of $|Z|_5$, d should be as large as possible, hence the deviation is higher for media with lower conductivity.

Hence, this novel approach combines rigorous mathematical analysis with experimental impedance spectral data, laying the foundation for a new kind of sensing methodology. Although at the current stage, the approach only allows for differentiation of cells in suspensions, it has the potential to be extrapolated and employed for monitoring of plant cell expressions in suspensions.

Received: 24 May 2021; Accepted: 9 September 2021

Published online: 29 September 2021

References

- Sophocleous, M., Karkotis, A. & Georgiou, J. A versatile, stand-alone system for a screen-printed, soil-sensing array for precision agriculture. *Proc. IEEE Sensors* **2020**, 23–26 (2020).
- Stafford, J. V. Implementing precision agriculture in the 21st century. *J. Agric. Eng. Res.* **76**, 267–275 (2000).
- Sophocleous, M., Contat-Rodrigo, L., Garcia-Breijo, E. & Georgiou, J. Towards solid-state, thick-film K^+ and Na^+ ion sensors for soil quality assessment. *Proc. IEEE Sensors* **2020**, 1–4 (2020).
- Zhang, N., Wang, M. & Wang, N. Precision agriculture—A worldwide overview. *Comput. Electron. Agric.* **36**, 113–132 (2002).
- Zarco-Tejada, J. P., Hubbard, N. & Loudjani, P. *Precision Agriculture: An opportunity for EU farmers—Potential Support with the CAP 2014–2020* (2014).
- Alexandratos, N. & Bruinsma, J. *World Agriculture Towards 2030/2050* (2012).
- Bongiovanni, R. & Lowenberg-Deboer, J. Precision agriculture and sustainability. *Precis. Agric.* **5**, 359–387 (2004).
- Sophocleous, M. & Georgiou, J. Precision agriculture: Challenges in sensors and electronics for real-time soil and plant monitoring. *2017 IEEE Biomed. Circuits Syst. Conf.* 1–4 (2017). <https://doi.org/10.1109/BIOCAS.2017.8325180>.
- Mahajan, U. & Bundel, B. R. Drones for Normalized Difference Vegetation Index (NDVI), to estimate crop health for precision agriculture: A cheaper alternative for spatial satellite sensors. *Anim. Sci. Biodivers. Ecol. Sci. Clim. Change* (2017).
- Sophocleous, M., Savva, P., Petrou, M. F., Atkinson, J. K. & Georgiou, J. A durable, screen-printed sensor for in-situ and real-time monitoring of concrete's electrical resistivity suitable for smart buildings/cities and IoT. *IEEE Sensors Lett.* (2018).
- Mouser Electronics. Arduino-Compatible Solutions (2017).
- Whalley, S. Smart sensors: The key to precision agricultural production (2016).
- Bar-on, L., Jog, A. & Shacham-Diamand, Y. Four Point Probe Electrical Spectroscopy Based System for Plant Monitoring. In *Proceedings of ISCAS 2019, Japan* 1–5 (2019). <https://doi.org/10.1109/iscas.2019.8702623>.
- Daponte, P. *et al.* A review on the use of drones for precision agriculture. *IOP Conf. Ser. Earth Environ. Sci.* **275**, 012022 (2019).
- Angelopoulou, T., Tziolas, N., Balafoutis, A., Zalidis, G. & Bochtis, D. Remote sensing techniques for soil organic carbon estimation: A review. *Remote Sens.* **11**, 1–18 (2019).
- Vermeulen, P. *et al.* Assessment of pesticide coating on cereal seeds by near infrared hyperspectral imaging. *J. Spectr. Imaging* **6**, 1–7 (2017).
- Sophocleous, M., Karkotis, A. & Georgiou, J. A versatile, stand-alone, in-field sensor node for implementation in precision agriculture. *IEEE J. Emerg. Sel. Top. Circuits Syst.* **3357** (2021).

18. Franks, W., Schenker, I., Schmutz, P. & Hierlemann, A. Impedance characterization and modeling of electrodes for biomedical applications. *IEEE Trans. Biomed. Eng.* **52**, 1295–1302 (2005).
19. Bertemes-Filho, P. & Simini, F. Bioimpedance in biomedical applications and research. *Bioimpedance Biomed. Appl. Res.* 1–279 (2018). <https://doi.org/10.1007/978-3-319-74388-2>.
20. Dean, D. A., Ramanathan, T., Machado, D. & Sundararajan, R. Electrical impedance spectroscopy study of biological tissues. *J. Electrostat.* **66**, 165–177 (2008).
21. Asami, K. & Yamaguchi, T. Dielectric spectroscopy of plant protoplasts. *Biophys. J.* **63**, 1493–1499 (1992).
22. Grossi, M. & Riccò, B. Electrical impedance spectroscopy (EIS) for biological analysis and food characterization: A review. *J. Sens. Sens. Syst.* **6**, 303–325 (2017).
23. Lin, C. M., Chen, L. H. & Chen, T. M. The development and application of an electrical impedance spectroscopy measurement system for plant tissues. *Comput. Electron. Agric.* **82**, 96–99 (2012).
24. Faisal, M. *et al.* Experimental investigation of innovative active packaging biofilms using electrical impedance spectroscopy. *J. Mol. Struct.* **1230**, 129648 (2021).
25. Zhang, M. I. N., Stout, D. G. & Willson, J. H. M. Electrical impedance analysis in plant tissues: Symplasmic resistance and membrane capacitance in the Hayden model. *J. Exp. Bot.* **41**, 371–380 (1990).
26. Zhang, M. I. N. & Willson, J. H. M. Electrical impedance analysis in plant tissues: A double shell model. *J. Exp. Bot.* **44**, 1369–1375 (1993).
27. Asami, K. Characterization of heterogeneous systems by dielectric spectroscopy. *Prog. Polym. Sci.* **27**, 1617–1659 (2002).
28. Asami, K., Hanai, T. & Koizumi, N. Dielectric properties of yeast cells. *J. Membr. Biol.* **28**, 169–180 (1976).
29. Matanguihan, R. M., Konstantinov, K. B. & Yoshida, T. Dielectric measurement to monitor the growth and the physiological states of biological cells. *Bioprocess Eng.* **11**, 213–222 (1994).
30. Soley, A. *et al.* On-line monitoring of yeast cell growth by impedance spectroscopy. *J. Biotechnol.* **118**, 398–405 (2005).
31. Cannizzaro, C., Gügerli, R., Marison, I. & Von Stockar, U. On-line biomass monitoring of CHO perfusion culture with scanning dielectric spectroscopy. *Biotechnol. Bioeng.* **84**, 597–610 (2003).
32. Asami, K. Characterization of biological cells by dielectric spectroscopy. *J. Non Cryst. Solids* **305**, 268–277 (2002).
33. Kadan-Jamal, K. *et al.* Electrical Impedance Spectroscopy of plant cells in aqueous biological buffer solutions and their modelling using a unified electrical equivalent circuit over a wide frequency range: 4 Hz to 20 GHz. *Biosens. Bioelectron.* (2020). <https://doi.org/10.1016/j.bios.2020.112485>.
34. Kadan-Jamal, K. *et al.* Electrical impedance spectroscopy of plant cells in aqueous buffer media over a wide frequency range of 4 Hz to 20 GHz. *Methods* **8**, 101185 (2021).
35. Koornneef, M., Hanhart, C. J. & Martinelli, L. A genetic analysis of cell culture traits in tomato. *Theor. Appl. Genet.* **74**, 633–641 (1987).
36. Nagata, T., Hasezawa, S. & Inze, D. When I encountered tobacco BY-2 cells! in *Tobacco BY-2 Cells. Biotechnology in Agriculture and Forestry*, vol. 53, 1–6 (Springer, 2004).
37. Murasnige, T. & Skoog, F. A Revised Medium for Rapid Growth and Bio Assays with Tobaoco Tissue Cultures.

Acknowledgements

The research was partially funded by the ministry of Science and Technology, Israel, Grant # 3-14345 titled “Single cell Sensor”. It was also partially supported by the Israel Science Foundation (Grant no. 1616/17). We would also like to acknowledge the Boris Mints Institute for Strategic Policy Solutions to Global Challenges, the Department of Public Policy and the Manna Centre for Food Security, Tel Aviv University for their generous support under the program “Plant based heat stress whole-cell-biosensor” (Grant no. 590351) 2017.

Author contributions

K.K.J. and A.J. contributed equally. K.K.J. performed the experiments. K.K.J., A.J., M.S. performed the data analysis. K.K.J., A.J., M.S., and Y.S.D. wrote the manuscript text. All authors reviewed the manuscript.

Competing interests

The authors declare no competing interests.

Additional information

Supplementary Information The online version contains supplementary material available at <https://doi.org/10.1038/s41598-021-98901-0>.

Correspondence and requests for materials should be addressed to K.K.-J.

Reprints and permissions information is available at www.nature.com/reprints.

Publisher’s note Springer Nature remains neutral with regard to jurisdictional claims in published maps and institutional affiliations.



Open Access This article is licensed under a Creative Commons Attribution 4.0 International License, which permits use, sharing, adaptation, distribution and reproduction in any medium or format, as long as you give appropriate credit to the original author(s) and the source, provide a link to the Creative Commons licence, and indicate if changes were made. The images or other third party material in this article are included in the article’s Creative Commons licence, unless indicated otherwise in a credit line to the material. If material is not included in the article’s Creative Commons licence and your intended use is not permitted by statutory regulation or exceeds the permitted use, you will need to obtain permission directly from the copyright holder. To view a copy of this licence, visit <http://creativecommons.org/licenses/by/4.0/>.

© The Author(s) 2021